Atmos. Chem. Phys., 25, 12451–12465, 2025
https://doi.org/10.5194/acp-25-12451-2025

Atmospheric Chemistry and Physics
Open Access
EGU

The critical role of volatile organic compound emissions in nitrate formation in Lhasa, Tibetan Plateau: insights from oxygen isotope anomaly measurements

Xueqin Zheng[1], Junwen Liu[1], Nima Chuduo[2], Bian Ba[2], Pengfei Yu[1], Phu Drolgar[2], Fang Cao[3], and Yanlin Zhang[3]

[1]College of Environment and Climate, Jinan University, Guangzhou, 511443, China
[2]Lhasa Meteorological Administration, Lhasa, 850010, China
[3]School of Ecology and Applied Meteorology, Nanjing University of Information Science and Technology, Nanjing, 210044, China

Correspondence: Junwen Liu (liu.junwen@jnu.edu.cn)

Received: 14 January 2025 – Discussion started: 7 March 2025
Revised: 13 June 2025 – Accepted: 11 July 2025 – Published: 9 October 2025

Abstract. Atmospheric particulate nitrate aerosol (NO_3^-), produced via the oxidation of nitrogen oxides ($NO_x = NO + NO_2$), plays an important role in atmospheric chemistry and air quality, yet its formation mechanism remains poorly constrained in the plateau region. In this study, we report for the first time the yearly variation in the signatures of the stable oxygen isotope anomaly ($\Delta^{17}O = \delta^{17}O - 0.52 \times \delta^{18}O$) in NO_3^- collected in the urban Lhasa (3650 meters above sea level (m a.s.l.)), on the Tibetan Plateau, China. Our results show that NO_2+OH was the largest contributor to NO_3^- formation (46±26 %), followed by NO_3+volatile organic compound (VOC) (26± 18 %) and $N_2O_5 + H_2O$ (28 ± 11 %) using the Bayesian Isotope Mixture Model. Notably, there were significant differences in the NO_2+OH, NO_3+VOC, and N_2O_5+H_2O pathways between spring and the other three seasons (T test, $p < 0.05$). Using the Hybrid Single-Particle Lagrangian Integrated Trajectory (HYSPLIT) dispersion model, we highlighted the influence of VOC emissions from regions such as Afghanistan and northern India, which enhanced NO_3^- concentrations in Lhasa during spring. Furthermore, the diurnal distribution of NO_3^- oxidation pathways varied distinctly across seasons, suggesting that these differences in NO_3^- pathways were attributed to aerosol liquid water content (ALWC), VOC concentrations, and the atmospheric lifetime of NO_3^-.

1 Introduction

Nitrate aerosol (NO_3^-) is a key component regulating the mass concentration of atmospheric fine particulate matter ($PM_{2.5}$), which is highly related to air quality (Colmer et al., 2020), public health (Zhang et al., 2019, 2017; Geng et al., 2021), and the climate system (Clark and Tilman, 2008). Globally, the mass contribution of NO_3^- in $PM_{2.5}$ is in the range of 5 %–30 % (Huang et al., 2014; Xu et al., 2019; Salameh et al., 2015; Espina-Martin et al., 2024; Bell et al., 2007; Sun et al., 2022), depending on the locations and the severities of air pollution. For example, it was reported that NO_3^- accounted for 22 %, 27 %, and 26 % of $PM_{2.5}$ in megacities in China (Zong et al., 2020), Europe (Espina-Martin et al., 2024), and the US (Sun et al., 2022), respectively. In addition, some studies found that the contribution of NO_3^- would increase by 3–8 times with the occurrence of the particle-derived haze pollution (Ge et al., 2024; Song et al., 2019; Yin et al., 2022; Walters et al., 2024).

It is well known that atmospheric NO_3^- is formed by the oxidation of nitrogen oxides ($NO_x = NO + NO_2$) with different oxidants such as O_3, OH, and RO_2 (Text S1 in the Supplement). In general, atmospheric chemical transportation models are employed to depict the detailed oxidation pathways of NO_3^- formation. However, there remains considerable uncertainty in modeling the contribution of individual oxidation

pathways to NO_3^- formation, particularly the $N_2O_5 + H_2O$ pathway, due to the wide variability of key parameters such as the N_2O_5 uptake coefficient, which has been shown to vary significantly depending on aerosol composition, relative humidity, and temperature. For example, it was reported that the predicted N_2O_5 uptake to NO_3^- formation in Beijing, as estimated using WRF-Chem, ranged from 5 % to 21 % (Su et al., 2017). Higher contributions between 66 % and 85 % have been observed when applying the CMAQ model in Beijing (Qiu et al., 2019). Therefore, the application of alternative techniques is crucial for providing more reliable estimates and enhancing our understanding of NO_3^- formation mechanisms, in addition to the insights gained from atmospheric chemical transportation models.

Stable oxygen isotope anomaly ($\Delta^{17}O = \delta^{17}O - 0.52 \times \delta^{18}O$) is recognized as a powerful tool to track the formation pathways of atmospheric NO_3^- (Zhang et al., 2024; Feng et al., 2023). This is because the oxygen atoms in the terminal positions of O_3 exhibit an elevated $\Delta^{17}O$ ($\Delta^{17}O = 39 \pm 2$‰) (Vicars and Savarino, 2014), whereas the $\Delta^{17}O$ values of other atmospheric oxidants (e.g., H_2O, OH, and RO_2) that can be incorporated into NO_3^- are very close to 0‰. (Dubey et al., 1997; Barkan and Luz, 2003; Alexander et al., 2020) Therefore, $\Delta^{17}O(NO_3^-)$ serves as a unique tracer of O_3 involvement in its formation pathways, offering valuable insights into the relative contributions of individual reactions. In recent years, the use of $\Delta^{17}O(NO_3^-)$ to elucidate NO_3^- formation has garnered considerable attention. Walters et al. (2024) reported that the major formation pathways of annual HNO_3 production in the northeastern US were $NO_2 + OH$ (46 %), N_2O_5 uptake (34 %), and organic nitrate hydrolysis (12 %), with notable seasonal variability. Additionally, Zhang et al. (2022) observed that the contribution of nocturnal chemistry to NO_3^- formation increased at night, peaking at 72 % around midnight. In contrast, the contribution of $NO_2 + OH$ rose with sunrise, reaching its highest fraction (48 %) around noon. However, nearly all current $\Delta^{17}O$-related observations have been conducted in the plain cities, with little attention given to plateau cities, where atmospheric conditions generally suffer from distinct energy consumption patterns and unique climatic factors (e.g., intense solar radiation). In this study, we present detailed results from comprehensive field observations conducted in Lhasa (3650 meters above sea level, m a.s.l.), one of the highest cities in the world, located on the Tibetan Plateau, China. For the first time, we quantify the relative contribution of three oxidation pathways to NO_3^- formation in Lhasa on the basis of ambient measurements for $\Delta^{17}O$ signatures in NO_3^-.

2 Materials and methods

2.1 Sampling campaign

$PM_{2.5}$ samples were collected on the roof of a building (~ 15 m above ground) at the Meteorological Bureau of Lhasa (91.08° E, 29.40° N; Fig. 1) in China. Lhasa, the capital of the Tibet Autonomous Region, is a rapidly developing city with a population of ~ 950 000 and an urban area of ~ 30 000 km^2 (Office of the Leading Group, 2025). The sampling site is surrounded by mixed land use, including residential areas, government offices, religious temples, and commercial zones, with minimal heavy industry. The strong solar radiation and large diurnal temperature variations in this sampling site can lead to pronounced changes in the boundary layer height, which in turn significantly influence vertical mixing and the transport of air pollutants.

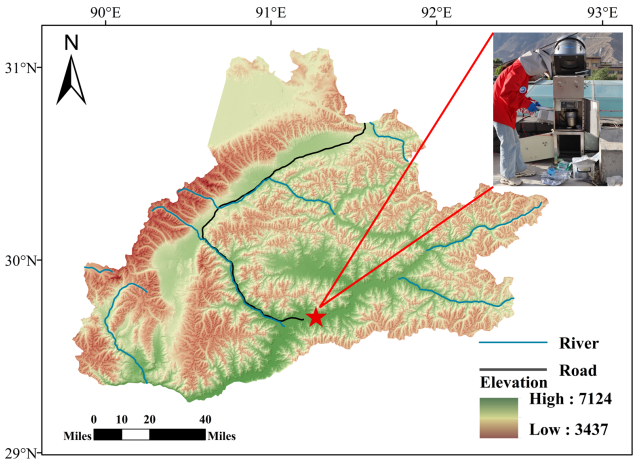

Figure 1. Geographic position of the sampling site in Lhasa, China.

The sampling campaign was conducted from June 2022 to July 2023 using a high-volume $PM_{2.5}$ sampler, which operated at a flow rate of 1.0 $m^3\,min^{-1}$. Samples were collected once a week, with each sampling session lasting 48 h, except during intensive sampling periods in the summer (30 June–14 July 2022) and winter (28 January–7 February 2023). During these intensive periods, each sample was collected for 12 h, from 8:00 to 20:00 LT and from 20:00 to 8:00 LT on the following day. During the autumn of 2022, Lhasa experienced intermittent COVID-19 control measures, including restricted movement, reduced traffic activity, and temporary lockdowns in urban areas (Lhasa Municipal People's Government, 2025). Before sampling, all quartz filters (8 in. × 10 in., i.e., 20.3 cm × 25.4 cm, Pallflex) were calcined in a muffle furnace at 450 °C for 6 h to prevent impurities from contaminating the collected $PM_{2.5}$ samples. After sampling, the samples were collected and stored in a freezer at −20 °C.

2.2 Measurements of water-soluble ions and isotopes

Water-soluble ions were measured by ion chromatography (Dionex ICS-5000, Thermo Scientific Inc.) (Chen et al., 2022). In brief, a part of the filter membranes (4.54 cm^2) was cut using a 17 mm diameter punch and placed in a 15 mL centrifuge tube with 10 mL of 18.2 MΩ ultrapure water. The

tube was then subjected to ultrasonic treatment in an ice-water bath for 30 min to prevent ion volatilization. The extract was filtered through a 0.22 µm filter into a 30 mL sample bottle. This process was repeated with an additional 10 mL of water to ensure full extraction. The final extract was analyzed by ion chromatography. The method detection limits (MDLs) for Cl^-, NO_3^-, SO_4^{2-}, Na^+, NH_4^+, K^+, Mg^{2+}, and Ca^{2+} were 0.001, 0.001, 0.003, 0.02, 0.01, 0.02, 0.006, and 0.02 mg L^{-1}, respectively.

Stable oxygen isotopes ($\delta^{17}O$, $\delta^{18}O$, $\Delta^{17}O$, and $\Delta^{17}O = \delta^{17}O - 0.52 \times \delta^{18}O$) of NO_3^- were determined using an isotope ratio mass spectrometer (MAT253, Thermo Fisher Scientific, USA) at Nanjing University of Information Science and Technology (Fan et al., 2021; Zhang et al., 2022). Briefly, NO_3^- from filter extractions (containing at least 0.8 µg N) was converted into gaseous N_2O using the bacterial denitrifier method. N_2O was then further thermally decomposed into O_2 and N_2 in a gold tube heated to 800 °C. The produced O_2 was analyzed for oxygen isotopes by an isotope ratio mass spectrometer. The duplicate analysis showed that the errors were within 1.32 % for $\Delta^{17}O{-}NO_3^-$.

2.3 Primary data sources

Meteorological parameters, including ambient temperature (T), relative humidity (RH), rainfall, radiation, wind direction (WD), and wind speed (WS) during the sampling campaign, were obtained from the Meteorological Bureau of Lhasa. Additionally, NO_2 and O_3 during the sampling campaign were downloaded from the National Meteorological Information Center (https://air.cnemc.cn:18007/, last access: 21 December 2023).

2.4 Evaluation of NO_3^- oxidation pathways

In our study, we aimed to quantify the relative contribution of different oxidation pathways to NO_3^- production based on $\Delta^{17}O{-}NO_3^-$. Due to the low Cl^- concentrations observed in Lhasa, the NO_3^- formation pathways considered in this study were limited to $NO_2 + OH$, NO_3 + volatile organic compound (VOC), and $N_2O_5 + H_2O$. Although NO_3 + VOC is generally considered a minor pathway in continental regions (Alexander et al., 2009), we included it because elevated VOC concentrations were observed at our sampling site in Lhasa, influenced by both biomass burning (e.g., incense burning) and anthropogenic sources (e.g., vehicle emissions) (Tang et al., 2022). The relative contributions of the three pathways were determined using a $\Delta^{17}O$-based mass balance approach (Michalski et al., 2003), as shown in Eqs. (1) and (2):

$$\begin{aligned}\Delta^{17}O{-}NO_3{}^- = {} & (\Delta^{17}O{-}NO_3^-)_{NO_2+OH} \\ & \times f_{NO_2+OH} + (\Delta^{17}O{-}NO_3^-)_{NO_3+VOC} \times f_{NO_3+VOC} \\ & + (\Delta^{17}O{-}NO_3^-)_{N_2O_5+H_2O} \times f_{N_2O_5+H_2O}\end{aligned} \quad (1)$$

$$f_{NO_2+OH} + f_{NO_3+VOC} + f_{N_2O_5+H_2O} = 1 \quad (2)$$

where $\Delta^{17}O{-}NO_3^-$ value is the $\Delta^{17}O$ value of NO_3^- in $PM_{2.5}$. The $(\Delta^{17}O{-}NO_3^-)_{NO_2+OH}$, $(\Delta^{17}O{-}NO_3^-)_{NO_3+VOC}$, and $(\Delta^{17}O{-}NO_3^-)_{N_2O_5+H_2O}$ correspond to the $\Delta^{17}O$ values from NO_2+OH, NO_3+VOC, and $N_2O_5+H_2O$, respectively. The $\Delta^{17}O$ values for each pathway were calculated using Eqs. (3)–(5) (Savarino et al., 2016; Alexander et al., 2009):

$$(\Delta^{17}O{-}NO_3^-)_{NO_2+OH}(‰) = \frac{2}{3}\alpha \times \Delta^{17}O{-}O_3^* \quad (3)$$

$$\begin{aligned}(\Delta^{17}O{-}NO_3^-)_{NO_3+VOC}(‰) = {} & \frac{2}{3}\alpha \times \Delta^{17}O{-}O_3^* \\ & + \frac{1}{3} \times \Delta^{17}O{-}O_3^*\end{aligned} \quad (4)$$

$$\begin{aligned}(\Delta^{17}O{-}NO_3^-)_{N_2O_5+H_2O}(‰) = {} & \frac{1}{3}\alpha \times \Delta^{17}O{-}O_3^* \\ & + \frac{1}{2}\left(\frac{2}{3}\alpha \times \Delta^{17}O{-}O_3^* + \frac{1}{3} \times \Delta^{17}O{-}O_3^*\right)\end{aligned} \quad (5)$$

Previous studies have demonstrated a linear correlation between $\Delta^{17}O{-}O_3$ and $\Delta^{17}O{-}O_3^*$ with $\Delta^{17}O{-}O_3$ values ranging from 20 % to 40 % in tropospheric O_3 (Vicars and Savarino, 2014; Ishino et al., 2017). The equations are shown as follows (Vicars et al., 2012):

$$\Delta^{17}O{-}O_3^* = 1.5 \times \Delta^{17}O{-}O_3 \quad (6)$$

Based on previous observations of tropospheric O_3, the $\Delta^{17}O{-}O_3^*$ average value was approximately 39 ‰. The α value represents the proportional contribution of O_3 to the NO oxidation pathway and can be estimated using the following Eqs. (7) (Alexander et al., 2009). When NO_x is in photochemical steady state, $\Delta^{17}O{-}NO_2$ can be represented using the following Eq. (10):

$$\alpha = \frac{K_{p1}[O_3] \times [NO]}{K_{p1}[O_3] \times [NO] + K_{p2}[HO_2] \times [NO] + K_{p3}[RO_2] \times [NO]} \quad (7)$$

$$K_{p1} = 3.0 \times 10^{-2} \times e^{\left(-\frac{1500}{T}\right)} \quad (8)$$

$$K_{p2} = K_{p3} = 3.5 \times 10^{-12} \times e^{\frac{270}{T}} \quad (9)$$

$$\Delta^{17}O{-}NO_2 = \alpha \times \Delta^{17}O{-}O_3^* \quad (10)$$

where T represents the ambient temperature (K) (Kunasek et al., 2008). The HO_2 mixing ratios were estimated using empirical equations in the absence of direct HO_2 observations (Kanaya et al., 2007). Due to the lower temperatures in Lhasa during non-summer seasons, HO_2 concentrations were assessed using a formula derived from winter conditions.

Winter

$$[HO_2]/ppt = \exp(5.7747 \times 10^{-2}[O_3](ppb) - 1.7227) \quad \text{for daytime} \tag{11}$$

$$[HO_2]/ppt = \exp(7.7234 \times 10^{-2}[O_3](ppb) - 1.6363) \quad \text{for nighttime} \tag{12}$$

Summer

$$[HO_2]/ppt = \exp(2.0706 \times 10^{-2}[O_3](ppb) + 1.0625) \quad \text{for daytime} \tag{13}$$

$$[HO_2]/ppt = 0.2456 + 0.1841[O_3](ppb) \quad \text{for nighttime} \tag{14}$$

2.5 Stable isotope analysis in the R (SIAR) model

In this study, stable isotope analysis in the R (SIAR) model was employed to estimate the relative contributions of three main pathways to NO_3^- (Parnell et al., 2010). The SIAR model is well-suited for analyzing multiple formation pathways, as it effectively incorporates uncertainties and parameter variability, leading to more reliable estimates. Specifically, this model allows for a detailed analysis of oxygen isotope ($\Delta^{17}O$), enabling accurate modeling of NO_3^- formation pathways based on oxygen isotope measurements. The SIAR model is a Bayesian mixture model, mathematically formulated as follows:

$$X_i = \sum_{j=1}^{K} p_j \times f_{ij}$$
$$p_1 + p_2 + \ldots + p_k = 1$$
$$f_{ij} \sim N(\mu_j, \omega_j^2)$$

where X_i is the observed $\Delta^{17}O$ value for sample i ($i = 1, 2, 3, \ldots, N$), and p_j is the proportional contribution of each NO_3^- formation pathway j to the sample i. f_{ij} is the $\Delta^{17}O$ value of formation pathway j for sample i and follows a normal distribution with mean (μ_j) and variance (ω_j^2). Within the Bayesian framework, prior distributions are assigned to each p_j, and these are updated with the observed data X_i to obtain posterior distributions, allowing for inference of the proportional contributions p_j of each pathway.

2.6 Aerosol liquid water content (ALWC) and the Hybrid Single-Particle Lagrangian Integrated Trajectory (HYSPLIT)

To evaluate the influence of ALWC on NO_3^- formation, ALWC was calculated using the ISORROPIA II model developed by Fountoukis and Nenes (Fountoukis and Nenes, 2007). The ISORROPIA II model includes two modes: the forward mode, which requires the concentrations of both particulate and gaseous pollutants as inputs, and the reverse mode, which only requires the concentrations of particulate pollutants. The model computes the ALWC in both modes based on particulate pollutant concentrations (e.g., NH_4^+, Na^+, Ca^{2+}, K^+, and Mg^{2+}), as well as ambient RH and T. In this study, the reverse mode was employed due to the lack of gaseous pollutant concentration observations.

Additionally, the Hybrid Single-Particle Lagrangian Integrated Trajectory (HYSPLIT) model was utilized to compute 72 h back trajectories during the sampling campaign. HYSPLIT, developed by the National Oceanic and Atmospheric Administration Air Resources Laboratory, is available on their website (https://www.ready.noaa.gov/HYSPLIT.php, last access: 1 December 2024). This model has been widely used for simulating the transport and dispersion trajectories of pollutants such as $PM_{2.5}$, VOC, O_3, and NO_x, among others (He et al., 2022; Zhao et al., 2015; Cao et al., 2023). Backward trajectories for each sampling day were calculated at an altitude of 3650 m using meteorological data from the Global Data Assimilation System (GDAS), available through the US Air Resources Laboratory (https://www.ready.noaa.gov/data/archives/gdas1/, last access: 15 December 2023).

3 Results

3.1 Overview of the meteorological parameters in Lhasa during the sampling campaign

Figure 2a presents the daily variations in meteorological parameters, including T, RH, rainfall, and solar radiation. During the sampling campaign, the annual average T was 11.5 °C, ranging from −2.83 to 24.2 °C. The highest average T was observed in summer (19.7 °C), while the lowest (3.11 °C) was recorded in winter. RH varied between 6.67 % and 66.8 %, with the lowest average RH occurring in winter (17.1 %) and the highest in summer (35.6 %). The near-surface layer of Lhasa is influenced by a thermal low-pressure system, and the southwest monsoon, active between June and September, transports moisture-laden air from the Indian Ocean, resulting in increased rainfall during summer. Solar radiation intensity exhibited a seasonal trend consistent with those of T and RH, peaking in summer (394 $W\,m^{-2}$) and reaching its lowest levels in winter (220 $W\,m^{-2}$). The dominant WD was southeast in spring and southwest in the other three seasons (Fig. 3). WS was highest in spring and lowest in autumn.

3.2 NO_3^- concentration

NO_3^- mass concentrations ranged from 0.10 to 1.72 $\mu g\,m^{-3}$, with an average value of $0.62 \pm 0.31\,\mu g\,m^{-3}$. NO_3^- concentrations exhibited distinct seasonal patterns. As shown in Fig. S1 in the Supplement, the equivalent concentrations of $[SO_4^{2-} + NO_3^-]$ were considerably higher than those of $[NH_4^+]$, indicating that NH_4^+ was insufficient to fully neutralize NO_3^-. This suggests that a portion of NO_3^- may have existed in other forms, such as KNO_3 and $Ca(NO_3)_2$. This

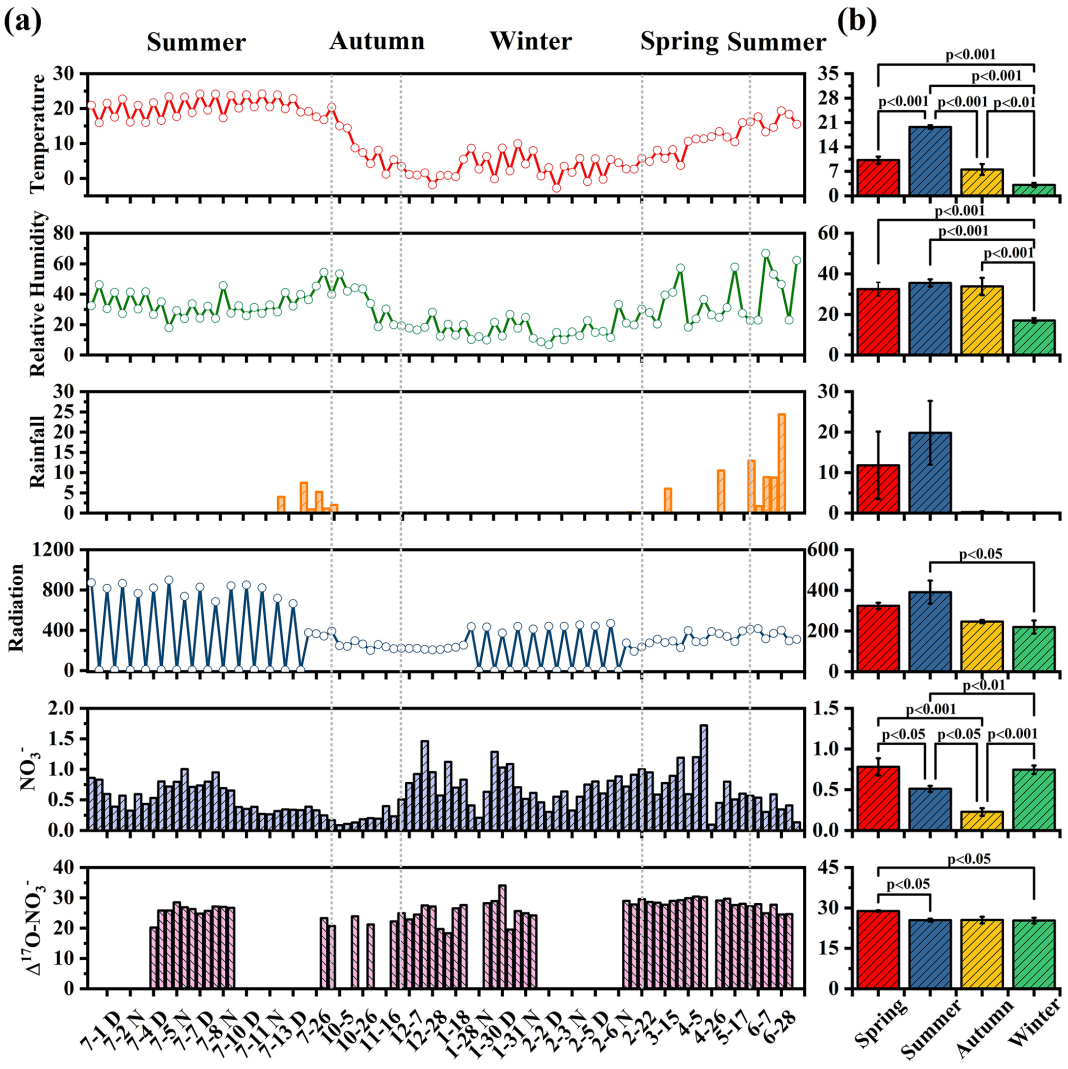

Figure 2. **(a)** shows the time series of temperature (°C), relative humidity (%), rainfall (mm), radiation ($W\,m^{-2}$), NO_3^- concentration ($\mu g\,m^{-3}$), and $\Delta^{17}O{-}NO_3^-$ (‰) from June 2022 to July 2023. **(b)** shows the average values at different seasons with their statistical significance.

inference is supported by the strong positive correlations between NO_3^- and K^+ ($r = 0.64$, $p < 0.1$) and Ca^{2+} ($r = 0.43$, $p < 0.01$), especially in spring, as shown in Fig. S2. In contrast, NO_3^- showed relatively weak negative correlations with T ($r = -0.27$, $p < 0.01$) and RH ($r = -0.22$, $p < 0.1$), indicating that under the specific atmospheric conditions in Lhasa, meteorological parameters might not be the dominant factors controlling the gas-particle partitioning of NO_3^-. The maximum monthly average values of NO_3^- concentration occurred in spring ($0.83 \pm 0.35\,\mu g\,m^{-3}$) with the instantaneous maximum reaching $1.72\,\mu g\,m^{-3}$, whereas the lowest was recorded in autumn ($0.23 \pm 0.13\,\mu g\,m^{-3}$) with an instantaneous minimum of only $0.09\,\mu g\,m^{-3}$ (Table 1). The elevated NO_3^- concentrations in spring could be attributed to biomass burning from South and Southeast Asia (Figs. S3 and S4). The strong correlation between NO_3^- and K^+ in spring further supports this explanation.

In spring, high NO_3^- concentrations were associated with weak southeasterly winds ($< 3\,m\,s^{-1}$) in the bivariate polar plot, suggesting probable impacts from local emissions (Fig. 3). The southeasterly sector of the sampling site includes residential areas, agricultural land, and major transportation routes, which are potential NO_x sources. In spring, intensified agricultural activities (e.g., fertilization, biomass burning) might increase NO_x emissions. Meanwhile, low wind speeds likely limit atmospheric dispersion, promoting the local accumulation of precursors and enhancing NO_3^- production. During the rainy summer, shorter NO_3^- lifetimes indicated a weak influence from regional transport, with a more pronounced contribution from local emissions. In autumn, NO_3^- concentrations were relatively low, which coin-

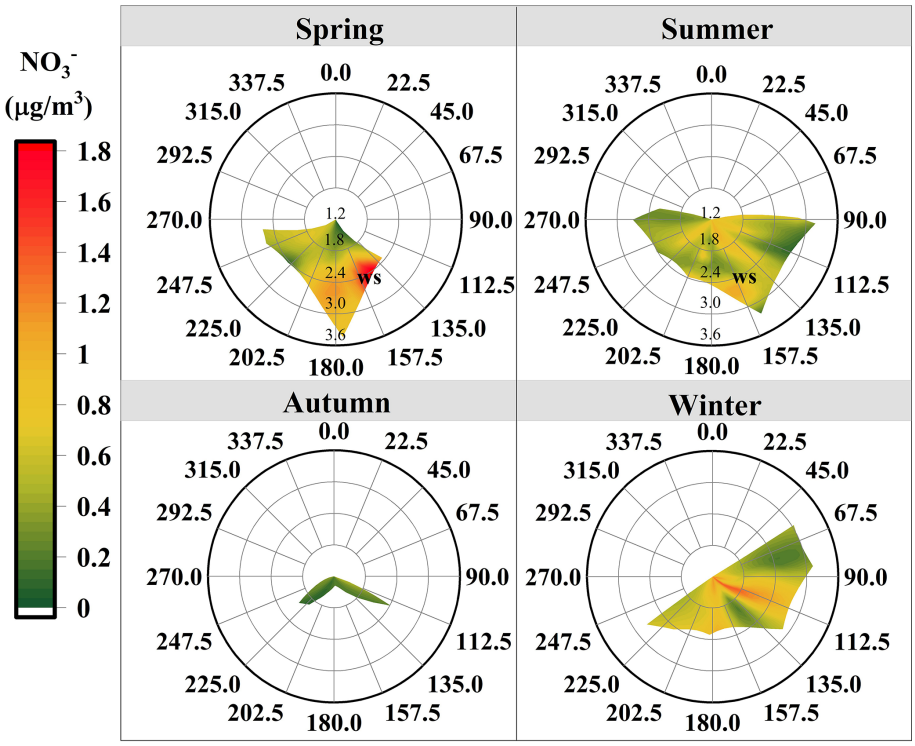

Figure 3. The bivariate polar plot illustrates the seasonal variation in the mass concentration of NO_3^- in relation to wind speed (WS, $m\,s^{-1}$) and wind direction (WD, degrees).

cided with strict local COVID-19 restrictions in Lhasa. These measures significantly reduced human activity and traffic, leading to suppressed local emissions. Despite low wind speeds typically favoring pollutant accumulation, NO_3^- concentrations remained low, suggesting that both reduced local sources and seasonal meteorological conditions constrained NO_3^- production. Nevertheless, the persistence of measurable NO_3^- under such stagnant conditions also implied a potential contribution from regional transport during this period. In winter, elevated NO_3^- concentrations under low wind speeds ($< 3\,m\,s^{-1}$) emphasized the significant contribution of local emissions. These findings underscored that both regional transport and local emissions were important contributors to NO_3^- concentrations in Lhasa. Furthermore, based on our day-night sampling scheme, no nychthemeral (day–night) differences in NO_3^- concentrations were detected (Table S1 in the Supplement). A similar day-night pattern of NO_3^- concentrations has also been observed in Beijing (Luo et al., 2020).

3.3 Oxygen isotopes of NO_3^-

To explore the three major oxidation pathways of NO_3^- formation, 53 samples representing varying NO_3^- concentrations across different seasons were selected for oxygen isotope measurements (Fig. 2b). The $\Delta^{17}O{-}NO_3^-$ values ranged from 18.3‰ to 34.1‰, with an average of 26.3 ± 3.13‰, which is slightly lower than the global average of 28.6 ± 4.5‰ simulated by the Global Chemical Transport Model (Alexander et al., 2020). As shown in Table S2, the observed $\Delta^{17}O{-}NO_3^-$ values in this study were similar to most mid- and low-latitude regions, but lower than those in polar regions (~ 32‰). As listed in Table S1, the average $\Delta^{17}O{-}NO_3^-$ values in spring, summer, autumn, and winter were 28.8 ± 8.0‰, 25.5 ± 2.20‰, 25.6 ± 1.35‰, and 25.9 ± 3.56‰, respectively. The differences in $\Delta^{17}O{-}NO_3^-$ values between spring and summer, as well as between spring and winter, were statistically significant ($p < 0.05$). The elevated $\Delta^{17}O{-}NO_3^-$ values in spring could be attributed to a higher proportion of nocturnal pathways that enrich $\Delta^{17}O{-}NO_3^-$ values, such as $NO_3 + VOC$ and $N_2O_5 + H_2O$ pathways. In contrast, the lower $\Delta^{17}O{-}NO_3^-$ values in the other three seasons suggested a greater production of NO_3^- formation via the $NO_2 + OH$ pathway, leading to more negative $\Delta^{17}O{-}NO_3^-$ values. Diurnal variation in $\Delta^{17}O{-}NO_3^-$ values also differed across seasons (Fig. S5). In summer, the average of $\Delta^{17}O{-}NO_3^-$ values during the day (25.3 ± 2.39‰) was lower than at night (26.7 ± 1.03‰). Conversely, in winter, the average of $\Delta^{17}O{-}NO_3^-$ values during the day (28.0 ± 3.79‰) was significantly higher than at night (24.4 ± 3.85‰). Similar diurnal patterns, with higher daytime $\Delta^{17}O{-}NO_3^-$ values and lower nighttime values, have also been observed in winter in the US (Vicars et al., 2013) and other cities in China (He et al., 2018).

Table 1. Average values of water-soluble ions and $\Delta^{17}O-NO_3^-$ during the sampling campaign.

		Na^+ $\mu g\,m^{-3}$	NH_4^+ $\mu g\,m^{-3}$	K^+ $\mu g\,m^{-3}$	Mg^{2+} $\mu g\,m^{-3}$	Ca^{2+} $\mu g\,m^{-3}$	Cl^- $\mu g\,m^{-3}$	NO_3^- $\mu g\,m^{-3}$	SO_4^{2-} $\mu g\,m^{-3}$	$\Delta^{17}O-NO_3^-$ ‰
Annual	Minimum	0.02	0	0.004	0.004	0.004	0.004	0.09	0.06	18.3
	Maximum	0.68	1.22	0.29	0.08	3.52	0.51	1.72	2.37	34.1
	Average	0.16	0.3	0.07	0.02	1.09	0.08	0.62	0.74	26.3
	Std. Dev.	0.14	0.26	0.06	0.01	0.7	0.1	0.31	0.45	3.13
Spring	Minimum	0.04	0.16	0.04	0.01	1.02	0.01	0.45	0.6	27.2
	Maximum	0.16	1.22	0.2	0.05	2.56	0.05	1.72	2.14	30.4
	Average	0.09	0.52	0.09	0.02	1.67	0.03	0.83	1.11	28.8
	Std. Dev.	0.03	0.3	0.04	0.01	0.51	0.01	0.35	0.52	0.99
Summer	Minimum	0.02	0	0.01	0.01	0.03	0.003	0.13	0.18	20.2
	Maximum	0.4	1.08	0.09	0.04	2.4	0.13	1	2.37	28.5
	Average	0.09	0.18	0.03	0.02	1.15	0.3	0.5	0.72	25.5
	Std. Dev.	0.08	0.17	0.02	0.01	0.5	0.3	0.23	0.45	2.2
Autumn	Minimum	0.02	0.003	0.004	0.01	0.004	0.01	0.09	0.06	21.2
	Maximum	0.17	0.11	0.1	0.03	0.24	0.17	0.51	0.55	24.9
	Average	0.09	0.04	0.3	0.02	0.13	0.05	0.23	0.31	23.05
	Std. Dev.	0.05	0.04	0.3	0.01	0.08	0.05	0.13	0.14	1.44
Winter	Minimum	0.06	0.09	0.02	0.01	0.05	0.04	0.21	0.32	18.3
	Maximum	0.56	0.87	0.29	0.08	3.52	0.51	1.46	1.57	34.1
	Average	0.19	0.44	0.12	0.03	1.04	0.16	0.75	0.73	25.9
	Std. Dev.	0.12	0.21	0.08	0.02	0.78	0.13	0.28	0.34	3.86

4 Discussion

4.1 A comparison of NO_3^- oxidation pathways in Lhasa with other megacities in plain regions

Typically, observations of $\Delta^{17}O-NO_3^-$ and estimated α (the proportion of O_3 oxidation in NO_2 production rate) values are employed to quantify the contributions of major NO_3^- oxidation pathways in conjunction with a Bayesian model. The α value ranged from 0.63 to 0.93, with an average of 0.83 ± 0.06, suggesting the significance of O_3 participation in NO oxidation during the sampling campaign. On the other hand, our α values were lower than those (0.85–1) for other midlatitude regions (Alexander et al., 2009). The α values are influenced by the relative amount of O_3, HO_2, and RO_2 in NO_x cycling. Due to the generally high O_3 concentrations ($O_3 > 50$ ppb) observed in Lhasa, nearly all α values exceeded 0.8 (Fig. S6). To evaluate the impact of key parameters on the estimated contributions of different NO_3^- formation pathways, we conducted a sensitivity analysis by assuming the α values and $\Delta^{17}O$ value of the terminal oxygen atoms of O_3 ($\Delta^{17}O-O_3^*$). As listed in Table S3, the assumptions of α and $\Delta^{17}O-O_3^*$ had an impact on the NO_3^- formation mechanisms. When $\Delta^{17}O-O_3^*$ was fixed at 39 ‰, increasing α from 0.7 to 0.9 led to a notable increase in the relative contribution of the $NO_2 + OH$ pathway from 25 % to 46 %, while that of the $NO_3 + VOC$ pathway decreased from 46 % to 25 %. The $N_2O_5 + H_2O$ pathway remained nearly constant, with contributions ranging between 28 % and 29 %, indicating that this pathway is relatively insensitive to changes in α values. Similarly, when α was varied within a reasonable range (0.68–0.93), increasing the $\Delta^{17}O-O_3^*$ value from 37 ‰ to 39 ‰ led to an increase in the $NO_2 + OH$ contribution from 37 % to 46 % and a corresponding decrease in the $NO_3 + VOC$ contribution from 35 % to 26 %. Again, the $N_2O_5 + H_2O$ contribution remained stable at ~ 28 %. These results suggest that the estimated contributions of $NO_2 + OH$ and $NO_3 + VOC$ pathways are sensitive to assumptions about α and $\Delta^{17}O-O_3^*$, whereas the contribution of the $N_2O_5 + H_2O$ pathway is relatively robust under the tested conditions. Because Lhasa is characterized by relatively high VOC concentrations and $\Delta^{17}O-O_3^*$ is generally close to 39 ‰, we consider our parameter assumptions reasonable for further estimating NO_3^- formation pathways for each sample.

On average, the relative contributions of $NO_2 + OH$ (f_{NO_2+OH}), $NO_3 + VOC$ (f_{NO_3+VOC}), and $N_2O_5 + H_2O$ ($f_{N_2O_5+H_2O}$) to NO_3^- formation in Lhasa during the sampling campaign were 46 ± 26 %, 26 ± 19 %, and 28 ± 11 %, respectively. To better understand the characteristics of NO_3^- formation mechanisms in Lhasa, we performed a detailed comparison across China for the relative contributions of key oxidation pathways using the $\Delta^{17}O$ methodology (Fig. 4). Overall, similar to most Chinese cities, NO_3^- formation in Lhasa was predominantly driven by the $NO_2 + OH$ pathway,

exhibiting distinct seasonal and regional variations. In particular, the average f_{NO_3+VOC} values were generally several times higher in spring in Lhasa than in other urban cities. Compared to rural/remote areas, the average f_{NO_3+VOC} values showed higher fractions in Lhasa, revealing the influence of anthropogenic emissions, i.e., vehicle exhaust and heating, on NO_3^- formation. In Lhasa, the capital of Tibet, field measurements over different years showed a substantial increase in VOC concentrations in urban areas of the Tibetan Plateau, comparable to those in North China (Tang et al., 2022), revealing the importance of the active $NO_3 + VOC$ pathway for NO_3^- pollution formation in Lhasa. In fact, recent studies have recognized $NO_3 + VOC$ as a major formation mechanism for NO_3^- production. For instance, Fan et al. (2021) found that the f_{NO_3+VOC} values in Beijing increased from 17 % in summer to 32 % in winter based on $\Delta^{17}O-NO_3^-$ measurements. He et al. (2018) estimated the f_{NO_2+OH} and f_{NO_3+VOC} values and found that they were in the range of 16 %–56 %, underscoring the significant roles of these pathways during haze events in Beijing. Similarly, Feng et al. (2023) also reported that the f_{NO_3+VOC} values were up to 49.6 % in winter in northern China. In Guangzhou, Wang et al. (2023) noted that the average f_{NO_3+VOC} value was at 488 m (25 %), which was higher than that at the ground (12 %). Furthermore, Li et al. (2022) reported that the f_{NO_3+VOC} values increased from 5 % in urban to 13.5 % in rural regions in Northeast China. Although the specific nighttime RO_2 production mechanism in Lhasa remains unclear, studies in other cities have demonstrated that the NO_3+VOC pathway was the dominant channel for nighttime RO_2 production (Fisher et al., 2016), which in turn led to the formation of alkyl and multifunctional nitrates ($RONO_2$) and eventually NO_3^-. In such cases, the RO_2 concentration is expected to be correlated with NO_3 radical production, which depends on the reaction rate of O_3 and NO_2 (Brown and Stutz, 2012). Given the relatively high nighttime O_3 concentrations in Lhasa, it is plausible that O_3-driven nighttime NO_3 chemistry plays an important role, thereby enhancing $NO_3 + VOC$ derived from RO_2 production and NO_3^- formation. Global modeling studies also support the significance of this pathway. For instance, Alexander et al. (2020) reported that the $NO_3 + VOC$ pathway via the $RONO_2$ mechanism accounted for 3 % of global NO_3^- formation on average. The relatively high f_{NO_3+VOC} values observed in Lhasa are broadly consistent with these findings, especially under conditions of high VOC concentrations and strong nighttime oxidant levels.

4.2 Seasonal and diurnal variations of NO_3^- oxidation pathways

Figure S7 illustrates the seasonal variations in the relative contributions of the three main oxidation pathways to NO_3^- formation. When comparing different seasons, the f_{NO_2+OH} values were lower ($p < 0.01$) in spring (22.6 %) than in winter (50.8 %), summer (52.9 %), and autumn (73.2 %). The dominance of the $NO_2 + OH$ pathway in autumn is consistent with observations at Mount Everest during the autumn season of 2017 and 2018, suggesting that NO_3^- formation on the Tibetan Plateau in autumn may be mainly driven by the $NO_2 + OH$ pathway (Lin et al., 2021; Wang et al., 2020b).

A significant increase in the f_{NO_3+VOC} values was observed in spring ($p < 0.05$). First, O_3 and NO_2 are precursors of NO_3. In this work, the highest concentrations of O_3 were found in spring ($114.9 \pm 18.1\,\mu g\,m^{-3}$), likely leading to elevated NO_3 concentrations. Additionally, the low T and reduced OH radical concentrations in spring facilitate the reaction of NO_2 and O_3 to synthesize NO_3. This might be an appropriate reason for the f_{NO_3+VOC} values in spring. High-altitude locations such as Nepal (5079 m a.s.l.) and Qomolangma Station (4300 m a.s.l.) have experienced stratospheric ozone intrusions, especially in spring and winter, as reported in previous studies (Zhang et al., 2025, 2022; Cristofanelli et al., 2010; Morin et al., 2007; Lin et al., 2016; Yin et al., 2017; Wang et al., 2020b). Notably, such intrusions in spring may elevate tropospheric O_3 levels in Lhasa, resulting in a mixture of tropospheric and stratospheric O_3 that enhances NO_3^- production. Second, previous studies have indicated that the Afghanistan–Pakistan–Tajikistan region, the Indo-Gangetic Plain, and the Meghalaya–Myanmar region could transport industrial VOC emissions to various zones in Tibet from west to east. Additionally, agricultural areas in northern India could contribute biomass burning-related VOC emissions to the middle-northern and eastern regions of Tibet (Li et al., 2017). During our sampling campaign, South and Southeast Asia air clusters were notably prevalent in the springtime, coinciding with intensive fire spots observed in Afghanistan, Pakistan, India, Nepal, and Bhutan (Figs. S3 and S4). These observations, combined with the prevailing South and Southeast Asia air mass trajectories in spring, strongly suggest that long-range transported VOCs from South Asia were delivered to Lhasa and likely participated in local NO_3^- production via the $NO_3 + VOC$ pathway. Moreover, recent studies have shown that ambient VOC concentrations in the urban areas on the Qinghai–Tibet Plateau were comparable to those in the North China Plain (Tang et al., 2022). The input of VOC emissions through long-range transport might further elevate VOC concentrations, thereby promoting NO_3^- formation via the $NO_3 + VOC$ pathway and contributing to the enhanced f_{NO_3+VOC} values observed in spring. While VOCs appear to play a dominant role in the process, it should be noted that other nitrogen species (e.g., NO, NO_2) associated with biomass burning emissions may also be transported over long distances and influence NO_3^- formation in Lhasa. These co-transported nitrogen compounds, although not directly quantified in this study, could further contribute to NO_3^- production in spring. Taken together, these findings provide strong evidence that long-range transport of biomass burning emissions, particu-

larly from South Asia, can substantially influence springtime NO_3^- formation in Lhasa.

Similarly, the $f_{N_2O_5+H_2O}$ values exhibited their highest contributions during spring, with significant seasonal differences ($p < 0.05$) except when compared to summer ($p > 0.05$). Typically, high RH enhances NO_3^- formation via the $N_2O_5 + H_2O$ pathway. However, studies have revealed that during sandstorm events, a significantly large N_2O_5 uptake coefficient was observed on urban aerosols in spring (Xia et al., 2019). In this study, the mean Ca^{2+} concentration in $PM_{2.5}$ was found to be the highest in spring, suggesting a possible role of dust in facilitating N_2O_5 uptake. Additionally, the $N_2O_5 + H_2O$ pathway has been reported to be promoted by elevated NO_3^- concentrations (Lin et al., 2021), which were also highest in spring. Therefore, the increased $f_{N_2O_5+H_2O}$ values during spring might be attributed to the combined effects of lower RH, elevated Ca^{2+} levels, and high NO_3^- concentrations.

Interestingly, distinct diurnal patterns of NO_3^- oxidation pathways were observed during the sampling campaign (Fig. 5). In summer, the $NO_2 + OH$ pathway showed a significantly higher contribution during the daytime (55.1 %) compared to nighttime (44.9 %), which is attributed to increased OH radical synthesis during longer days and higher temperatures in Lhasa (Rohrer and Berresheim, 2006). A previous study indicated that lower NO_2 and higher O_3 concentrations enhance the relative contribution of the OH pathway to NO_3^- formation (Wang et al., 2019). Additionally, the concentration of ALWC (the detailed information is given in Text S3) was higher at night than during the day in summer, favoring NO_3^- formation through nocturnal formation. In winter, f_{NO_2+OH}, f_{NO_3+VOC}, and $f_{N_2O_5+H_2O}$ were similar during both day and night. Typically, photolytic destruction and chemical reactions with NO are rapid sinks during the daytime, with lifetimes generally less than 5 s, resulting in extremely low concentrations. Similarly, the atmospheric lifetime of N_2O_5 under sunlight is also very short (Wang et al., 2018). Thus, daytime NO_3 and N_2O_5 chemistry is often considered negligible. However, a recent study revealed that a non-negligible amount of NO_3 radicals can persist during the daytime in cold months, owing to the limited solar radiation (Hellén et al., 2018). Wang et al. (2020a) found that the daytime production rate of NO_3 can be substantial due to elevated concentrations of O_3 and NO_2, suggesting that the mixing ratios of NO_3 and N_2O_5 during the day may not be negligible. Furthermore, in winter, lower temperatures and elevated NO_2 concentrations facilitate a quasi-steady-state equilibrium between NO_3 and N_2O_5, slowing the overall reactivity of the NO_3^- precursors (Brown et al., 2003). This equilibrium condition minimizes diurnal fluctuations in precursor concentrations, resulting in relatively stable nocturnal and daytime NO_3^- formation pathways, including NO_3+VOC and N_2O_5+H_2O. Nevertheless, we acknowledge that the exact role of daytime NO_3/N_2O_5 chemistry remains uncertain in Lhasa and should be further assessed using concurrent field observations or chemical transport models. Moreover, when interpreting the diurnal differences in $\Delta^{17}O-NO_3^-$ values, the atmospheric lifetime of NO_3^- must be considered. Given that the atmospheric lifetime of NO_3^- is generally more than 12 h, each sample might reflect both daytime and nighttime NO_3^- production impacting $\Delta^{17}O-NO_3^-$ values (Park et al., 2004; Vicars et al., 2013).

4.3 Integrated analysis of NO_3^- oxidation pathways in Lhasa

As shown in Fig. S8, the $NO_3 + VOC$ pathway emerged as the major contributor to NO_3^- formation during periods of high NO_3^- spikes. To elucidate the NO_3^- formation pathways under different NO_3^- concentrations, NO_3^- samples were categorized into different concentration ranges (Fig. 6). We found that the f_{NO_3+VOC} values increased and f_{NO_2+OH} values decreased with the NO_3^- concentrations increasing. Although recent field radical measurements in urban sites in China found that OH and HO_2 radicals during haze periods were comparable to those on clean days (Slater et al., 2020; Yang et al., 2021), our results suggested that the $NO_3 + VOC$ pathway still played an important role in NO_3^- production under high NO_3^- concentrations in Lhasa, possibly due to enhanced VOC emissions. In addition to concentration effects, meteorological factors typically also regulate the NO_3^- oxidation pathways. Typically, high T promotes the NO_3^- formation via f_{NO_2+OH} values (Han et al., 2015). However, our study revealed that the relationship between T and f_{NO_2+OH} values did not consistently show a positive trend. Further analysis indicated that NO_2 and O_3 concentrations were negatively correlated, with lower NO_2 concentrations paired with elevated O_3 levels (Fig. S9). f_{NO_2+OH} values reached their minimum when NO_2 was between 15 and 20 $\mu g\,m^{-3}$ and O_3 was within 100–120 $\mu g\,m^{-3}$. Although OH radicals exhibit a higher oxidation potential (2.8 V) than O_3 (2.07 V), their atmospheric availability is much lower than that of O_3 (Carslaw et al., 1999; Dubey et al., 1997). Therefore, NO_2 at lower concentrations is more likely to be oxidized by OH than by O_3, even though O_3 concentrations were high. With increasing NO_2 concentrations, the availability of OH radicals for oxidizing NO_2 became lower, resulting in a relatively higher proportion of NO_2 being oxidized by O_3 although O_3 concentrations were low. However, when the concentration of O_3 was below 20 $\mu g\,m^{-3}$, O_3 concentrations were not sufficient to oxidize NO_2 due to the higher NO_2 concentrations and OH radicals for oxidizing NO_2 would redominate. These observations underscore that in high-altitude urban environments like Lhasa, OH effectiveness is more important for NO_3^- oxidation pathways than that of O_3. Additionally, we identified an intriguing positive correlation between the atmospheric oxidizing capacity ($O_x = NO_2 + O_3$) and f_{NO_3+VOC} values. f_{NO_3+VOC} values were lowest when O_x was less than 90 $\mu g\,m^{-3}$, corresponding to a maximum contribution from the $NO_2 + OH$ pathway. This suggests that

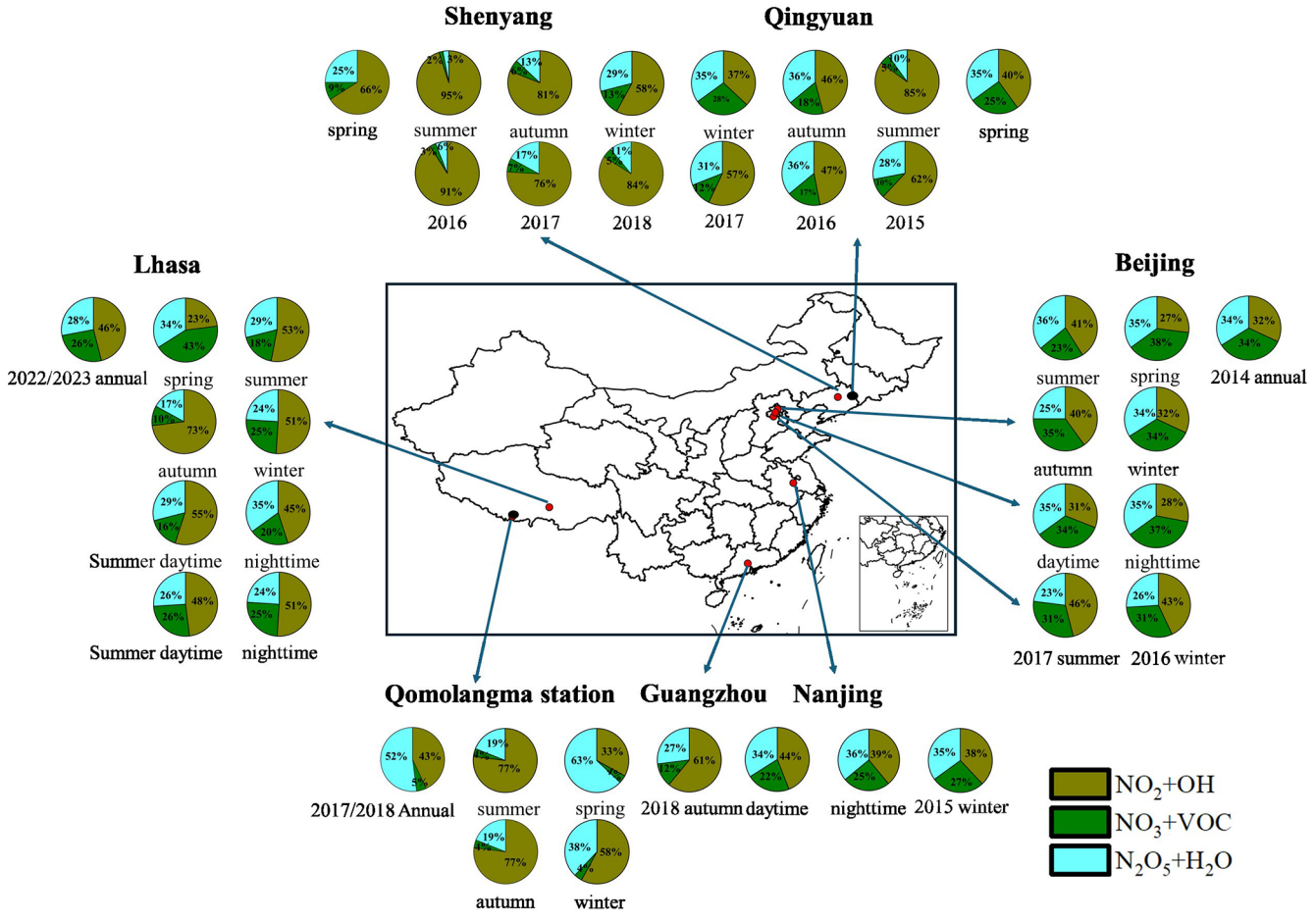

Figure 4. Summary of the relative contributions of key oxidation pathways using the $\Delta^{17}O$ methodology across China (data given in Table S4). Colors for the study labels indicate the type of sampling location: urban areas (red) and rural/remote areas (black). The pie charts show the relative contribution of different pathways to NO_3^- formation: f_{NO_2+OH} (deep yellow), f_{NO_3+VOC} (deep green), and $f_{N_2O_5+H_2O}$ (light blue).

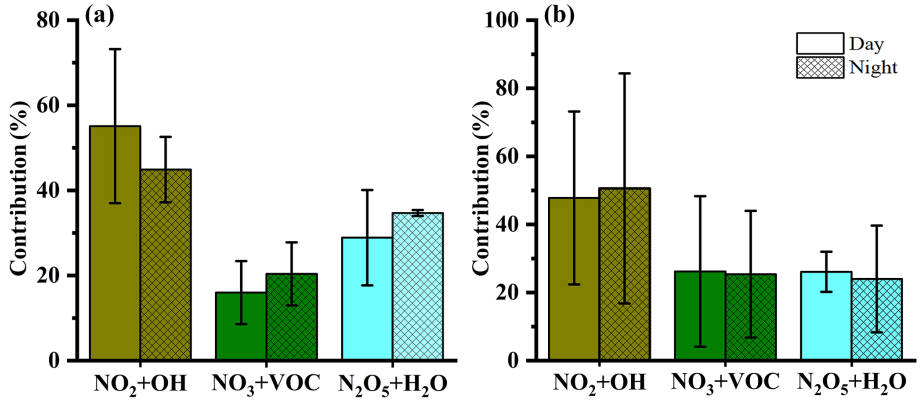

Figure 5. The relative contributions (mean ± SD values) of $NO_2 + OH$, $NO_3 + VOC$, and $N_2O_5 + H_2O$ to NO_3^- formation during the day and night in **(a)** summer and **(b)** winter in Lhasa during the sampling campaign.

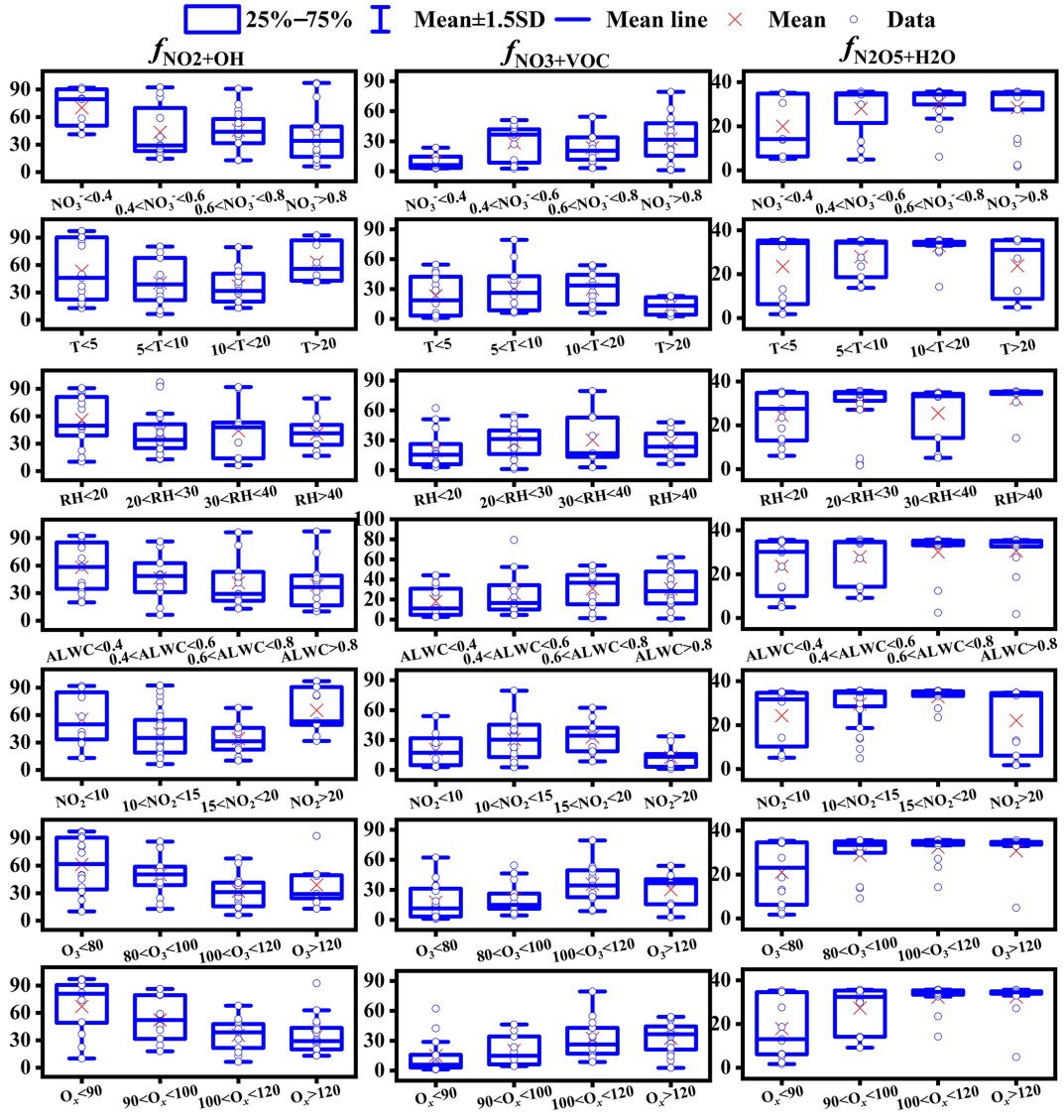

Figure 6. Influence of NO_3^- ($\mu g\,m^{-3}$), temperature (°C), RH (%), ALWC ($\mu g\,m^{-3}$), NO_2 ($\mu g\,m^{-3}$), O_3, and O_x ($\mu g\,m^{-3}$) on NO_3^- formation pathways (%).

O_x is more indicative of the pathways of NO_3^- formation in the atmosphere compared to either NO_2 or O_3 alone. Typically, high RH and ALWC were also positively correlated with $f_{N_2O_5+H_2O}$. However, RH was associated with variable contributions from the $N_2O_5 + H_2O$ pathway in our study, while increasing ALWC significantly enhanced this pathway, indicating ALWC as a more reliable indicator of NO_3^- formation.

4.4 Implications

The oxidation pathways of NO_3^- in Lhasa, China, were constrained using a full year of $\Delta^{17}O{-}NO_3^-$ measurements from 2022 to 2023. Based on seasonal data, we observed a significant increase in the relative contribution of the NO_3+VOC to NO_3^- formation during spring. Furthermore, the diurnal distribution of NO_3^- oxidation pathways varied distinctly across seasons. To better understand the factors influencing these pathways, we integrated meteorological conditions, NO_x precursors, and ALWC for a more comprehensive analysis of NO_3^- formation. The results revealed that O_x and ALWC were more reliable indicators of NO_3^- oxidation pathways than meteorological factors. Notably, Lhasa's unique high-altitude environment, such as strong solar radiation, persistently high O_3, and elevated VOC, promotes active NO_3 + VOC chemistry, especially in spring. Atmospheric ALWC is primarily produced by hygroscopic aerosols such as SO_4^{2-}, NH_4^+, and Cl^-. Therefore, in addition to controlling NO_2, O_3, and VOC, reducing these hygroscopic aerosols is crucial for effective $PM_{2.5}$ pollution control.

Although this study provides valuable insights into NO_3^- formation mechanisms in Lhasa, we must acknowledge the associated uncertainties due to the lack of comprehensive observational constraints in Lhasa. Specifically, the limited understanding of local RO_2 concentrations led us to adopt empirical parameterizations and refer to measurements from other regions, which inevitably introduced uncertainty into the pathway apportionment. In addition, the absence of direct observations of nighttime NO emissions and the NO_2–NO isotope exchange processes in this region further complicates the interpretation of diurnal variations in NO_3^- formation pathways. To improve the robustness of $\Delta^{17}O$-based pathway analysis, future studies should consider synchronous measurements of both NO_2 and NO_3^- isotopes.

Data availability. All data are presented in the main text and/or the Supplement. For additional data, please contact the corresponding author (liu.junwen@jnu.edu.cn).

Supplement. The supplement related to this article is available online at https://doi.org/10.5194/acp-25-12451-2025-supplement.

Author contributions. JL designed, conceived, and led the research. XZ performed the data analysis and drafted the manuscript. JL, XZ, NC, and BB planned and carried out the measurements. NC, BB, and PD were responsible for measuring the meteorological parameters. JL and PY secured funding for the continuous aerosol sampling and analysis. FC and YZ provided expertise on isotope analysis methods. JL offered guidance on data analysis, and all authors contributed to revising the manuscript.

Competing interests. The contact author has declared that none of the authors has any competing interests.

Disclaimer. Publisher's note: Copernicus Publications remains neutral with regard to jurisdictional claims made in the text, published maps, institutional affiliations, or any other geographical representation in this paper. While Copernicus Publications makes every effort to include appropriate place names, the final responsibility lies with the authors.

Financial support. This study was supported by the Natural Science Foundation of Xizang Autonomous Region (XZ202401ZR0067), Guangdong Basic and Applied Basic Research Foundation (2024B1515040026), the second Tibetan Plateau Scientific Expedition and Research Program (20190ZKK0604), and the Guangdong Provincial General Colleges and Universities Innovation Team Project (Natural Science) (2024KCXTD004).

Review statement. This paper was edited by Lisa Whalley and reviewed by two anonymous referees.

References

Alexander, B., Hastings, M. G., Allman, D. J., Dachs, J., Thornton, J. A., and Kunasek, S. A.: Quantifying atmospheric nitrate formation pathways based on a global model of the oxygen isotopic composition ($\Delta^{17}O$) of atmospheric nitrate, Atmos. Chem. Phys., 9, 5043–5056, https://doi.org/10.5194/acp-9-5043-2009, 2009.

Alexander, B., Sherwen, T., Holmes, C. D., Fisher, J. A., Chen, Q., Evans, M. J., and Kasibhatla, P.: Global inorganic nitrate production mechanisms: comparison of a global model with nitrate isotope observations, Atmos. Chem. Phys., 20, 3859–3877, https://doi.org/10.5194/acp-20-3859-2020, 2020.

Barkan, E. and Luz, B.: High-precision measurements of $^{17}O/^{16}O$ and $^{18}O/^{16}O$ of O_2 and O_2 Ar^{-1} ratio in air, Rapid Commun. Mass Sp., 17, 2809–2814, https://doi.org/10.1002/rcm.1267, 2003.

Bell, M. L., Dominici, F., Ebisu, K., Zeger, S. L., and Samet, J. M.: Spatial and temporal variation in $PM_{2.5}$ chemical composition in the United States for health effects studies, Environ. Health Persp., 115, 989–995, https://doi.org/10.1289/ehp.9621, 2007.

Brown, S. S. and Stutz, J.: Nighttime radical observations and chemistry, Chem. Soc. Rev., 41, 6405–6447, https://doi.org/10.1039/C2CS35181A, 2012.

Brown, S. S., Stark, H., and Ravishankara, A.: Applicability of the steady state approximation to the interpretation of atmospheric observations of NO_3 and N_2O_5, J. Geophys. Res.-Atmos., 108, https://doi.org/10.1029/2011JD016544, 2003.

Cao, X., Xing, Q., Hu, S., Xu, W., Xie, R., Xian, A., Xie, W., Yang, Z., and Wu, X.: Characterization, reactivity, source apportionment, and potential source areas of ambient volatile organic compounds in a typical tropical city, J. Environ. Sci., 123, 417–429, https://doi.org/10.1016/j.jes.2022.08.005, 2023.

Carslaw, N., Creasey, D. J., Heard, D. E., Lewis, A. C., McQuaid, J. B., Pilling, M. J., Monks, P. S., Bandy, B. J., and Penkett, S. A.: Modeling OH, HO_2, and RO_2 radicals in the marine boundary layer: 1. Model construction and comparison with field measurements, J. Geophys. Res.-Atmos., 104, 30241–30255, https://doi.org/10.1029/1999JD900783, 1999.

Chen, Z., Pei, C., Liu, J., Zhang, X., Ding, P., Dang, L., Zong, Z., Jiang, F., Wu, L., and Sun, X.: Non-agricultural source dominates the ammonium aerosol in the largest city of South China based on the vertical $\delta^{15}N$ measurements, Sci. Total Environ., 848, 157750, https://doi.org/10.1016/j.scitotenv.2022.157750, 2022.

Clark, C. M. and Tilman, D.: Loss of plant species after chronic low-level nitrogen deposition to prairie grasslands, Nature, 451, 712–715, https://doi.org/10.1038/nature06503, 2008.

Colmer, J., Hardman, I., Shimshack, J., and Voorheis, J.: Disparities in $PM_{2.5}$ air pollution in the United States, Science, 369, 575–578, https://doi.org/10.1126/science.aaz9353, 2020.

Cristofanelli, P., Bracci, A., Sprenger, M., Marinoni, A., Bonafè, U., Calzolari, F., Duchi, R., Laj, P., Pichon, J. M., Roccato, F., Venzac, H., Vuillermoz, E., and Bonasoni, P.: Tropospheric ozone variations at the Nepal Climate Observatory-Pyramid (Himalayas, 5079 m a.s.l.) and influence of deep strato-

spheric intrusion events, Atmos. Chem. Phys., 10, 6537–6549, https://doi.org/10.5194/acp-10-6537-2010, 2010.

Dubey, M. K., Mohrschladt, R., Donahue, N. M., and Anderson, J. G.: Isotope specific kinetics of hydroxyl radical (OH) with water (H_2O): Testing models of reactivity and atmospheric fractionation, J. Phys. Chem. A, 101, 1494–1500, https://doi.org/doi/abs/10.1021/jp962332p, 1997.

Espina-Martin, P., Perdrix, E., Alleman, L., and Coddeville, P.: Origins of the seasonal variability of $PM_{2.5}$ sources in a rural site in Northern France, Atmos. Environ., 120660, https://doi.org/10.1016/j.atmosenv.2024.120660, 2024.

Fan, M.-Y., Zhang, Y.-L., Lin, Y.-C., Hong, Y., Zhao, Z.-Y., Xie, F., Du, W., Cao, F., Sun, Y., and Fu, P.: Important role of NO_3 radical to nitrate formation aloft in urban Beijing: Insights from triple oxygen isotopes measured at the tower, Environ. Sci. Technol., 56, 6870–6879, https://doi.org/10.1021/acs.est.1c02843, 2021.

Feng, X., Chen, Y., Chen, S., Peng, Y., Liu, Z., Jiang, M., Feng, Y., Wang, L., Li, L., and Chen, J.: Dominant Contribution of NO_3 Radical to NO_3^- Formation during Heavy Haze Episodes: Insights from High-Time Resolution of Dual Isotopes $\Delta^{17}O$ and $\delta^{18}O$, Environ. Sci. Technol., 57, 20726–20735, https://doi.org/10.1021/acs.est.3c07590, 2023.

Fisher, J. A., Jacob, D. J., Travis, K. R., Kim, P. S., Marais, E. A., Chan Miller, C., Yu, K., Zhu, L., Yantosca, R. M., Sulprizio, M. P., Mao, J., Wennberg, P. O., Crounse, J. D., Teng, A. P., Nguyen, T. B., St. Clair, J. M., Cohen, R. C., Romer, P., Nault, B. A., Wooldridge, P. J., Jimenez, J. L., Campuzano-Jost, P., Day, D. A., Hu, W., Shepson, P. B., Xiong, F., Blake, D. R., Goldstein, A. H., Misztal, P. K., Hanisco, T. F., Wolfe, G. M., Ryerson, T. B., Wisthaler, A., and Mikoviny, T.: Organic nitrate chemistry and its implications for nitrogen budgets in an isoprene- and monoterpene-rich atmosphere: constraints from aircraft ($SEAC^4RS$) and ground-based (SOAS) observations in the Southeast US, Atmos. Chem. Phys., 16, 5969–5991, https://doi.org/10.5194/acp-16-5969-2016, 2016.

Fountoukis, C. and Nenes, A.: ISORROPIA II: a computationally efficient thermodynamic equilibrium model for K^+–Ca^{2+}–Mg^{2+}–NH_4^+–Na^+–SO_4^{2-}–NO_3^-–Cl^-–H_2O aerosols, Atmos. Chem. Phys., 7, 4639–4659, https://doi.org/10.5194/acp-7-4639-2007, 2007.

Ge, S., Su, J., Zhao, P., Li, J., Liu, S., Qiu, Y., Pu, W., and Ma, Z.: Characteristics of $PM_{2.5}$ hygroscopicity and the influences of water-soluble ions during haze events in Beijing, Atmos. Environ., 322, 120382, https://doi.org/10.1016/j.atmosenv.2024.120382, 2024.

Geng, G., Zheng, Y., Zhang, Q., Xue, T., Zhao, H., Tong, D., Zheng, B., Li, M., Liu, F., and Hong, C.: Drivers of $PM_{2.5}$ air pollution deaths in China 2002–2017, Nat. Geosci., 14, 645–650, https://doi.org//10.1038/s41561-021-00792-3, 2021.

Han, T., Liu, X., Zhang, Y., Qu, Y., Zeng, L., Hu, M., and Zhu, T.: Role of secondary aerosols in haze formation in summer in the Megacity Beijing, J. Environ. Sci., 31, 51–60, https://doi.org/10.1016/j.jes.2014.08.026, 2015.

He, P., Xie, Z., Chi, X., Yu, X., Fan, S., Kang, H., Liu, C., and Zhan, H.: Atmospheric $\Delta^{17}O$ (NO_3^-) reveals nocturnal chemistry dominates nitrate production in Beijing haze, Atmos. Chem. Phys., 18, 14465–14476, https://doi.org/10.5194/acp-18-14465-2018, 2018.

He, S., Huang, M., Zheng, L., Chang, M., Chen, W., Xie, Q., and Wang, X.: Seasonal variation of transport pathways and potential source areas at high inorganic nitrogen wet deposition sites in southern China, J. Environ. Sci., 114, 444–453, https://doi.org/10.1016/j.jes.2021.12.024, 2022.

Hellén, H., Praplan, A. P., Tykkä, T., Ylivinkka, I., Vakkari, V., Bäck, J., Petäjä, T., Kulmala, M., and Hakola, H.: Long-term measurements of volatile organic compounds highlight the importance of sesquiterpenes for the atmospheric chemistry of a boreal forest, Atmos. Chem. Phys., 18, 13839–13863, https://doi.org/10.5194/acp-18-13839-2018, 2018.

Huang, R.-J., Zhang, Y., Bozzetti, C., Ho, K.-F., Cao, J.-J., Han, Y., Daellenbach, K. R., Slowik, J. G., Platt, S. M., and Canonaco, F.: High secondary aerosol contribution to particulate pollution during haze events in China, Nature, 514, 218–222, https://doi.org/10.1038/nature13774, 2014.

Ishino, S., Hattori, S., Savarino, J., Jourdain, B., Preunkert, S., Legrand, M., Caillon, N., Barbero, A., Kuribayashi, K., and Yoshida, N.: Seasonal variations of triple oxygen isotopic compositions of atmospheric sulfate, nitrate, and ozone at Dumont d'Urville, coastal Antarctica, Atmos. Chem. Phys., 17, 3713–3727, https://doi.org/10.5194/acp-17-3713-2017, 2017.

Kanaya, Y., Cao, R., Akimoto, H., Fukuda, M., Komazaki, Y., Yokouchi, Y., Koike, M., Tanimoto, H., Takegawa, N., and Kondo, Y.: Urban photochemistry in central Tokyo: 1. Observed and modeled OH and HO_2 radical concentrations during the winter and summer of 2004, J. Geophys. Res.-Atmos., 112, https://doi.org/10.1029/2007JD008670, 2007.

Kunasek, S., Alexander, B., Steig, E., Hastings, M., Gleason, D., and Jarvis, J.: Measurements and modeling of $\Delta^{17}O$ of nitrate in snowpits from Summit, Greenland, J. Geophys. Res.-Atmos., 113, https://doi.org/10.1029/2008JD010103, 2008.

Lhasa Municipal People's Government: Overview of Lhasa, https://www.lasa.gov.cn/lasa/yxls/yx.shtml, last access: 30 June 2025.

Li, H., He, Q., Song, Q., Chen, L., Song, Y., Wang, Y., Lin, K., Xu, Z., and Shao, M.: Diagnosing Tibetan pollutant sources via volatile organic compound observations, Atmos. Environ., 166, 244–254, https://doi.org/10.1016/j.atmosenv.2017.07.031, 2017.

Li, Z., Walters, W. W., Hastings, M. G., Song, L., Huang, S., Zhu, F., Liu, D., Shi, G., Li, Y., and Fang, Y.: Atmospheric nitrate formation pathways in urban and rural atmosphere of Northeast China: Implications for complicated anthropogenic effects, Environ. Pollut., 296, 118752, https://doi.org/10.1016/j.envpol.2021.118752, 2022.

Lin, M., Zhang, Z., Su, L., Hill-Falkenthal, J., Priyadarshi, A., Zhang, Q., Zhang, G., Kang, S., Chan, C. Y., and Thiemens, M. H.: Resolving the impact of stratosphere-to-troposphere transport on the sulfur cycle and surface ozone over the Tibetan Plateau using a cosmogenic ^{35}S tracer, J. Geophys. Res.-Atmos., 121, 439–456, https://doi.org/10.1002/2015JD023801, 2016.

Lin, Y.-C., Zhang, Y.-L., Yu, M., Fan, M.-Y., Xie, F., Zhang, W.-Q., Wu, G., Cong, Z., and Michalski, G.: Formation mechanisms and source apportionments of airborne nitrate aerosols at a Himalayan-Tibetan Plateau site: Insights from nitrogen and oxygen isotopic compositions, Environ. Sci. Technol., 55, 12261–12271, https://doi.org/10.1021/acs.est.1c03957, 2021.

Luo, L., Kao, S., Wu, Y., Zhang, X., Lin, H., Zhang, R., and Xiao, H.: Stable oxygen isotope constraints on nitrate forma-

tion in Beijing in springtime, Environ. Pollut., 263, 114515, https://doi.org/10.1016/j.envpol.2020.114515, 2020.

Michalski, G., Scott, Z., Kabiling, M., and Thiemens, M. H.: First measurements and modeling of $\Delta^{17}O$ in atmospheric nitrate, Geophys. Res. Lett., 30, https://doi.org/10.1029/2003GL017015, 2003.

Morin, S., Savarino, J., Bekki, S., Gong, S., and Bottenheim, J. W.: Signature of Arctic surface ozone depletion events in the isotope anomaly ($\Delta^{17}O$) of atmospheric nitrate, Atmos. Chem. Phys., 7, 1451–1469, https://doi.org/10.5194/acp-7-1451-2007, 2007.

Office of the Leading Group: Lhasa reported 31 new local COVID-19 cases yesterday, with 14 medium-risk areas adjusted, https://xinwen.bjd.com.cn/content/s6340d130e4b0b60bbc5d4ecd.html, last access: 1 July 2025.

Park, R. J., Jacob, D. J., Field, B. D., Yantosca, R. M., and Chin, M.: Natural and transboundary pollution influences on sulfate-nitrate-ammonium aerosols in the United States: Implications for policy, J. Geophys. Res.-Atmos., 109, https://doi.org/10.1029/2003JD004473, 2004.

Parnell, A. C., Inger, R., Bearhop, S., and Jackson, A. L.: Source partitioning using stable isotopes: coping with too much variation, PLoS One, 5, e9672, https://doi.org/10.1371/journal.pone.0009672, 2010.

Qiu, X., Ying, Q., Wang, S., Duan, L., Zhao, J., Xing, J., Ding, D., Sun, Y., Liu, B., Shi, A., Yan, X., Xu, Q., and Hao, J.: Modeling the impact of heterogeneous reactions of chlorine on summertime nitrate formation in Beijing, China, Atmos. Chem. Phys., 19, 6737–6747, https://doi.org/10.5194/acp-19-6737-2019, 2019.

Rohrer, F. and Berresheim, H.: Strong correlation between levels of tropospheric hydroxyl radicals and solar ultraviolet radiation, Nature, 442, 184–187, https://doi.org/10.1038/nature04924, 2006.

Salameh, D., Detournay, A., Pey, J., Pérez, N., Liguori, F., Saraga, D., Bove, M. C., Brotto, P., Cassola, F., and Massabò, D.: $PM_{2.5}$ chemical composition in five European Mediterranean cities: A 1 year study, Atmos. Res., 155, 102–117, https://doi.org/10.1016/j.atmosres.2014.12.001, 2015.

Savarino, J., Vicars, W. C., Legrand, M., Preunkert, S., Jourdain, B., Frey, M. M., Kukui, A., Caillon, N., and Gil Roca, J.: Oxygen isotope mass balance of atmospheric nitrate at Dome C, East Antarctica, during the OPALE campaign, Atmos. Chem. Phys., 16, 2659–2673, https://doi.org/10.5194/acp-16-2659-2016, 2016.

Slater, E. J., Whalley, L. K., Woodward-Massey, R., Ye, C., Lee, J. D., Squires, F., Hopkins, J. R., Dunmore, R. E., Shaw, M., Hamilton, J. F., Lewis, A. C., Crilley, L. R., Kramer, L., Bloss, W., Vu, T., Sun, Y., Xu, W., Yue, S., Ren, L., Acton, W. J. F., Hewitt, C. N., Wang, X., Fu, P., and Heard, D. E.: Elevated levels of OH observed in haze events during wintertime in central Beijing, Atmos. Chem. Phys., 20, 14847–14871, https://doi.org/10.5194/acp-20-14847-2020, 2020.

Song, W., Wang, Y.-L., Yang, W., Sun, X.-C., Tong, Y.-D., Wang, X.-M., Liu, C.-Q., Bai, Z.-P., and Liu, X.-Y.: Isotopic evaluation on relative contributions of major NO_x sources to nitrate of $PM_{2.5}$ in Beijing, Environ. Pollut., 248, 183–190, https://doi.org/10.1016/j.envpol.2019.01.081, 2019.

Su, X., Tie, X., Li, G., Cao, J., Huang, R., Feng, T., Long, X., and Xu, R.: Effect of hydrolysis of N_2O_5 on nitrate and ammonium formation in Beijing China: WRF-Chem model simulation, Sci. Total Environ., 579, 221–229, https://doi.org/10.1016/j.scitotenv.2016.11.125, 2017.

Sun, P., Farley, R. N., Li, L., Srivastava, D., Niedek, C. R., Li, J., Wang, N., Cappa, C. D., Pusede, S. E., and Yu, Z.: $PM_{2.5}$ composition and sources in the San Joaquin Valley of California: A long-term study using ToF-ACSM with the capture vaporizer, Environ. Pollut., 292, 118254, https://doi.org/10.1016/j.envpol.2021.118254, 2022.

Tang, G., Yao, D., Kang, Y., Liu, Y., Liu, Y., Wang, Y., Bai, Z., Sun, J., Cong, Z., Xin, J., Liu, Z., Zhu, Z., Geng, Y., Wang, L., Li, T., Li, X., Bian, J., and Wang, Y.: The urgent need to control volatile organic compound pollution over the Qinghai-Tibet Plateau, iScience, 25, 105688, https://doi.org/10.1016/j.isci.2022.105688, 2022.

Vicars, W., Morin, S., Savarino, J., Wagner, N., Erbland, J., Vince, E., Martins, J., Lerner, B., Quinn, P., and Coffman, D.: Spatial and diurnal variability in reactive nitrogen oxide chemistry as reflected in the isotopic composition of atmospheric nitrate: Results from the CalNex 2010 field study, J. Geophys. Res.-Atmos., 118, 10567–510588, https://doi.org/10.1002/jgrd.50680, 2013.

Vicars, W. C. and Savarino, J.: Quantitative constraints on the ^{17}O-excess ($\Delta^{17}O$) signature of surface ozone: Ambient measurements from 50 N to 50 S using the nitrite-coated filter technique, Geochim. Cosmochim. Ac., 135, 270–287, https://doi.org/10.1016/j.gca.2014.03.023, 2014.

Vicars, W. C., Bhattacharya, S., Erbland, J., and Savarino, J.: Measurement of the ^{17}O-excess ($\Delta^{17}O$) of tropospheric ozone using a nitrite-coated filter, Rapid Commun. Mass Sp., 26, 1219–1231, https://doi.org/10.1002/rcm.6218, 2012.

Walters, W. W., Pye, H. O., Kim, H., and Hastings, M. G.: Modeling the Oxygen Isotope Anomaly ($\Delta^{17}O$) of Reactive Nitrogen in the Community Multiscale Air Quality Model: Insights into Nitrogen Oxide Chemistry in the Northeastern United States, ACS ES&T Air, https://doi.org/10.1021/acsestair.3c00056, 2024.

Wang, H., Lu, K., Guo, S., Wu, Z., Shang, D., Tan, Z., Wang, Y., Le Breton, M., Lou, S., Tang, M., Wu, Y., Zhu, W., Zheng, J., Zeng, L., Hallquist, M., Hu, M., and Zhang, Y.: Efficient N_2O_5 uptake and NO_3 oxidation in the outflow of urban Beijing, Atmos. Chem. Phys., 18, 9705–9721, https://doi.org/10.5194/acp-18-9705-2018, 2018.

Wang, H., Chen, X., Lu, K., Hu, R., Li, Z., Wang, H., Ma, X., Yang, X., Chen, S., Dong, H., Liu, Y., Fang, X., Zeng, L., Hu, M., and Zhang, Y.: NO_3 and N_2O_5 chemistry at a suburban site during the EXPLORE-YRD campaign in 2018, Atmos. Environ., 224, 117180, https://doi.org/10.1016/j.atmosenv.2019.117180, 2020a.

Wang, K., Hattori, S., Kang, S., Lin, M., and Yoshida, N.: Isotopic constraints on the formation pathways and sources of atmospheric nitrate in the Mt. Everest region, Environ. Pollut., 267, 115274, https://doi.org/10.1016/j.envpol.2020.115274, 2020b.

Wang, Y., Liu, J., Jiang, F., Chen, Z., Wu, L., Zhou, S., Pei, C., Kuang, Y., Cao, F., and Zhang, Y.: Vertical measurements of stable nitrogen and oxygen isotope composition of fine particulate nitrate aerosol in Guangzhou city: Source apportionment and oxidation pathway, Sci. Total Environ., 865, 161239, https://doi.org/10.1016/j.scitotenv.2022.161239, 2023.

Wang, Y. L., Song, W., Yang, W., Sun, X. C., Tong, Y. D., Wang, X. M., Liu, C. Q., Bai, Z. P., and Liu, X. Y.: Influences of atmospheric pollution on the contributions of major oxidation pathways to $PM_{2.5}$ nitrate formation in Beijing, J. Geophys. Res.-Atmos., 124, 4174–4185, https://doi.org/10.1029/2019JD030284, 2019.

Xia, M., Wang, W., Wang, Z., Gao, J., Li, H., Liang, Y., Yu, C., Zhang, Y., Wang, P., Zhang, Y., Bi, F., Cheng, X., and Wang, T.: Heterogeneous Uptake of N_2O_5 in Sand Dust and Urban Aerosols Observed during the Dry Season in Beijing, Atmosphere, 10, 204, https://doi.org/10.3390/atmos10040204, 2019.

Xu, Q., Wang, S., Jiang, J., Bhattarai, N., Li, X., Chang, X., Qiu, X., Zheng, M., Hua, Y., and Hao, J.: Nitrate dominates the chemical composition of $PM_{2.5}$ during haze event in Beijing, China, Sci. Total Environ., 689, 1293–1303, https://doi.org/10.1016/j.scitotenv.2019.06.294, 2019.

Yang, X., Lu, K., Ma, X., Liu, Y., Wang, H., Hu, R., Li, X., Lou, S., Chen, S., and Dong, H.: Observations and modeling of OH and HO_2 radicals in Chengdu, China in summer 2019, Sci. Total Environ., 772, 144829, https://doi.org/10.1016/j.scitotenv.2020.144829, 2021.

Yin, M., Guan, H., Luo, L., Xiao, H., and Zhang, Z.: Using nitrogen and oxygen stable isotopes to analyze the major NO_x sources to nitrate of $PM_{2.5}$ in Lanzhou, northwest China, in winter-spring periods, Atmos. Environ., 276, 119036, https://doi.org/10.1016/j.atmosenv.2022.119036, 2022.

Yin, X., Kang, S., de Foy, B., Cong, Z., Luo, J., Zhang, L., Ma, Y., Zhang, G., Rupakheti, D., and Zhang, Q.: Surface ozone at Nam Co in the inland Tibetan Plateau: variation, synthesis comparison and regional representativeness, Atmos. Chem. Phys., 17, 11293–11311, https://doi.org/10.5194/acp-17-11293-2017, 2017.

Zhang, Q., Jiang, X., Tong, D., Davis, S. J., Zhao, H., Geng, G., Feng, T., Zheng, B., Lu, Z., Streets, D. G., Ni, R., Brauer, M., van Donkelaar, A., Martin, R. V., Huo, H., Liu, Z., Pan, D., Kan, H., Yan, Y., Lin, J., He, K., and Guan, D.: Transboundary health impacts of transported global air pollution and international trade, Nature, 543, 705–709, https://doi.org/10.1038/nature21712, 2017.

Zhang, Q., Zheng, Y., Tong, D., Shao, M., Wang, S., Zhang, Y., Xu, X., Wang, J., He, H., and Liu, W.: Drivers of improved $PM_{2.5}$ air quality in China from 2013 to 2017, P. Natl. Acad. Sci. USA, 116, 24463–24469, https://doi.org/10.1073/pnas.1907956116, 2019.

Zhang, Y., Zhao, T., Ning, G., Xu, X., Chen, Z., Jia, M., Sun, X., Shu, Z., Lu, Z., and Liu, J.: A unique mechanism of ozone surges jointly triggered by deep stratospheric intrusions and the Tibetan Plateau topographic forcing, Geophys. Res. Lett., 52, e2024GL114207, https://doi.org/10.1029/2024GL114207, 2025.

Zhang, Y.-L., Zhang, W., Fan, M.-Y., Li, J., Fang, H., Cao, F., Lin, Y.-C., Wilkins, B. P., Liu, X., and Bao, M.: A diurnal story of $\Delta^{17}O(NO_3^-)$ in urban Nanjing and its implication for nitrate aerosol formation, npj Climate and Atmospheric Science, 5, 50, https://doi.org/10.1038/s41612-022-00273-3, 2022.

Zhang, Z., Jiang, Z., Zhou, T., and Geng, L.: Reconciling Modeled and Observed $\Delta^{17}O(NO_3^-)$ in Beijing Winter Haze With Heterogeneous Chlorine Chemistry, J. Geophys. Res.-Atmos., 129, e2023JD039740, https://doi.org/10.1029/2023JD039740, 2024.

Zhao, M., Huang, Z., Qiao, T., Zhang, Y., Xiu, G., and Yu, J.: Chemical characterization, the transport pathways and potential sources of $PM_{2.5}$ in Shanghai: Seasonal variations, Atmos. Res., 158, 66–78, https://doi.org/10.1016/j.atmosres.2015.02.003, 2015.

Zong, Z., Tan, Y., Wang, X., Tian, C., Li, J., Fang, Y., Chen, Y., Cui, S., and Zhang, G.: Dual-modelling-based source apportionment of NOx in five Chinese megacities: Providing the isotopic footprint from 2013 to 2014, Environ. Int., 137, 105592, https://doi.org/10.1016/j.envint.2020.105592, 2020.